A Two Compartment Model of a CA1 Pyramidal Neuron

Katie A. Ferguson*†and Sue Ann Campbell ‡§

1 Introduction

Focal epilepsy is a neurological disorder which affects approximately 50 million people of all ages worldwide (World Health Organization, 2009). It is identified by recurrent unprovoked seizures, which are characterized by the excessive discharge (and often synchronization) of a large group of neurons in the brain. A simple, biologically relevant mathematical model would be helpful to examine the dynamics involved in these excessive discharges. Therefore we created a two-compartment mathematical model (based on a reduction of Traub et al.'s (1991) 19-compartment model) of a pyramidal neuron in the CA1 region of the hippocampus, a region which is often associated with seizure activity (Andersen et al., 2007; Traynelis and Dingledine, 1988). We model the communication between neurons through an AMPA synapse, which according to Traub et al. (1991) is the dominant method of synchronization amongst the neurons. Using our model, we reproduce behaviour of the 19-compartment model of Traub (1991) and of experiments.

2 Single Cell Model

Traub et al. (1991) created a 19-compartment model of a CA1 pyramidal neuron, and used their model to simulate key characteristics of a CA1 neuron. However, a more simplified model may be useful to examine the effects of key parameters, to create a network model, or to reduce the computational demand in order to extend the model in other ways. To reduce the number of compartments in the model, we noted that the CA1 neuron exhibited trains of action potentials when a small current ($< 1\ nA$) was applied to the soma, but a full calcium spike and burst followed by trains of action potentials when the same small current was applied to the distal dendrites (0.6λ from soma) (Traub et al., 1991). Thus we recognized the importance of distinguishing between the electrical properties in different parts of the neuron. This required the spatial separation of different channel types and the proper current flow between them (Traub et al., 1991). We concluded our model needed at least two compartments.

To construct these compartments we observed that the ionic channels were segregated such that their conductance strength varied significantly in the distal dendrites compared to the proximal dendrites and the somatic compartment (Traub et al., 1991). Therefore we used the general approach of Pinsky and Rinzel (1994): we lumped Traub's soma and proximal dendrite compartments into one soma compartment, and the distal dendrite compartments into one dendrite compartment. To determine which ion currents dominated in each compartmental region, we examined the non-unique distribution of ion channel conductance densities determined by Traub et al. (1991). Since we maintained the same volume/area ratio as Traub, and Traub's compartments had a length of 0.1λ, this gave our lumped compartments a length greater than 0.5λ. Thus,

*Department of Physiology, University of Toronto, Toronto ON
†Toronto Western Research Institute, University Health Network, Toronto ON
‡Department of Applied Mathematics, University of Waterloo, Waterloo ON N2L 3G1
§Corresponding author. Email:sacampbell@uwaterloo.ca

as for Pinsky & Rinzel's CA3 neuron model, our model should be considered as phenomenological rather than physiological.

A schematic representation of our model is given in Figure 1. The schematic shows the ionic currents present in each compartment, with the direction of current flow represented by an arrow. The applied currents ($I_D,\ I_S$) are shown, as well as the synaptic current (I_{SYN}). The two compartments are connected through the coupling parameters g_C, the strength of coupling, and p, the percentage of the cell model's total area taken up by the somatic compartment. The difference in potential across the membrane is denoted by V_S and V_D for the somatic and dendritic compartments respectively, and represents the deviation (in mV) from the resting membrane potential of $-60\ mV$. The somatic compartment has five ionic current channels: sodium and calcium are the inward currents ($I_{Na,S}$ and $I_{Ca,S}$ respectively), and the outward currents are the delayed rectifier potassium current ($I_{K-DR,S}$), long-duration calcium-dependent AHP potassium current ($I_{K-AHP,S}$), and short-duration voltage and calcium-dependent potassium ($I_{K-C,S}$). The dendrite compartment has three ionic current channels: an inward calcium current ($I_{Ca,D}$), and the outward $I_{K-AHP,D}$ and $I_{K-C,D}$. Although not shown in the schematic, there is a small leak current in both the soma and dendrite compartments. We use C_m to represent the membrane capacitance in units $\mu F/cm^2$. All currents in this model have the unit $\mu A/cm^2$ and all conductances have the unit mS/cm^2.

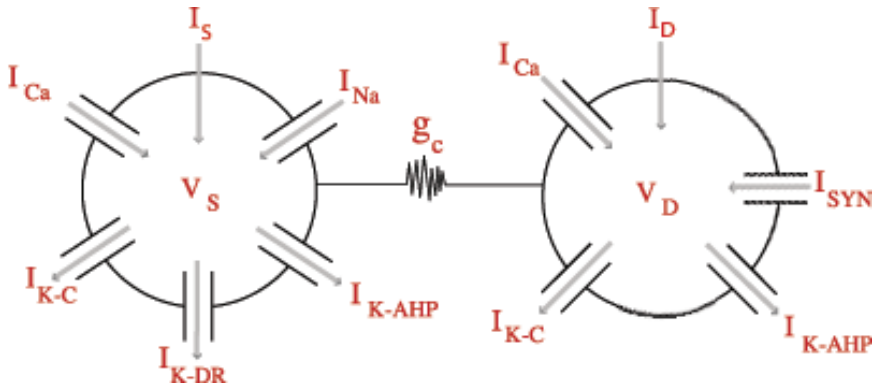

Figure 1: A schematic representation of our two-compartment CA1 neuron model.

The ionic currents are modeled as a function of their maximal conductance strengths and their corresponding Hodgkin-Huxley-like gating variables. The voltage dependent currents are given by:

$$
\begin{aligned}
I_{leak,j}(V_j) &= \bar{g}_{leak,j}(V_j - V_{leak}) && (1)\\
I_{Na,j}(V_j, h_j) &= \bar{g}_{Na,j} m_\infty^2(V_j) h_j (V_j - V_{Na}) && (2)\\
I_{K-DR}(V_j, n_j) &= \bar{g}_{K-DR,j} n_j (V_j - V_K) && (3)\\
I_{Ca,j}(V_j, s_j) &= \bar{g}_{Ca,j} s_j^2 (V_j - V_{Ca}) && (4)\\
& && (5)
\end{aligned}
$$

where $j \in \{S, D\}$, V_S and V_D are the membrane potentials for the somatic and dendritic compartments respectively. Sodium has an activation variable, m, and an inactivation variable, h. Since sodium activates almost instantaneously compared to the other variables, its activation variable is represented by the steady state value of m, m_∞, which is voltage dependent.

The activation for K-C and K-AHP ion channels depends on the calcium concentration inside the cell. Following standard practice (Traub et al., 1991), we model only the intracellular calcium

concentration in a "shell" beneath the cell membrane, given by the variables $[Ca^{2+}]_S$ and $[Ca^{2+}]_D$. The variation of each concentration is described by a simple production/degradation model:

$$\frac{d[Ca^{2+}]_j}{dt} = -\phi I_{Ca,j} - \beta_{[Ca^{2+}]}[Ca^{2+}]_j, \qquad j \in \{S, D\}$$

where ϕ is the scaling constant (with arbitrary units) that converts the inward calcium current to the internal calcium concentration.

We then have

$$\begin{aligned} I_{K-AHP,j}(V_j, q_j) &= \bar{g}_{K-AHP,j} q_j (V_j - V_K) \\ \text{and} \\ I_{K-C,j}(V_j, [Ca^{2+}]_j, c_j) &= \bar{g}_{K-C,j} \cdot c_j \cdot min(1, \frac{[Ca^{2+}]_j}{250}) \cdot (V_j - V_K) \end{aligned}$$

where $j \in \{S, D\}$.

The gating variables h_j, n_j, s_j, c_j, q_j, $j \in \{S, D\}$, are each governed by an equation of the form

$$\frac{dy_j}{dt} = \frac{y_\infty(U) - y_j}{\tau_y(U)}, \quad \text{with} \quad U = \begin{cases} V_j & \text{for } y_j \neq q_j \\ [Ca^{2+}]_j & \text{for } y_j = q_j \end{cases}.$$

The associated steady state value and time constant are defined in the usual manner

$$y_\infty(U) = \frac{\alpha_y(U)}{\alpha_y(U) + \beta_y(U)} \quad \text{and} \quad \tau_y(U) = \frac{1}{\alpha_y(U) + \beta_y(U)},$$

with rate constants as given in Traub et al. (1991):

$$\begin{aligned} \alpha_m(V_j) &= \frac{0.32 \times (13.1 - V_j)}{e^{(13.1-V_j)/4} - 1}, & \beta_m(V_j) &= \frac{0.28 \times (V_j - 40.1)}{e^{(V_j-40.1)/5} - 1} \\ \alpha_h(V_j) &= 0.128 \times e^{(17-V_j)/18}, & \beta_h(V_j) &= \frac{4}{e^{(40-V_j)/5} + 1} \\ \alpha_n(V_j) &= \frac{0.016 \times (35.1 - V_j)}{e^{(35.1-V_j)/5} - 1}, & \beta_n(V_j) &= 0.25 \times e^{(0.5-0.025V_j)} \\ \alpha_s(V_j) &= \frac{1.6}{1 + e^{-0.072\times(V_j-65)}}, & \beta_s(V_j) &= \frac{0.02 \times (V_j - 51.1)}{e^{(V_j-51.1)/5} - 1} \end{aligned}$$

$$\begin{aligned} \alpha_c(V_j) &= \begin{cases} 2 \times e^{(6.5-V_j)/27} & \text{if } V_j > 50 \\ (e^{\{((V_j-10)/11)-((V_j-6.5)/27)\}})/18.975 & \text{otherwise} \end{cases} \\ \beta_c(V_j) &= \begin{cases} 0 & \text{if } V_j > 50 \\ 2 \times e^{(6.5-V_j)/27} - \alpha_c(V_j) & \text{otherwise} \end{cases} \\ \alpha_q([Ca^{2+}]_j) &= \min(0.00002 \times [Ca^{2+}]_j, 0.01) \\ \beta_q &= 0.001 \end{aligned}$$

The synaptic current through AMPA receptor channels is given by I_{AMPA}. Then using Kirchoff's Law, we obtain an expression for the voltage change across the membrane of each compartment:

$$\frac{dV_S}{dt} = \frac{1}{C_m}\Big\{ - I_{leak,S}(V_S) - I_{Na,S}(V_S, h_S) - I_{K-DR,S}(V_S, n_S) - I_{Ca,S}(V_S, s_S) - I_{K-C,S}(V_S, [Ca^{2+}]_S, c_S) - I_{K-AHP,S}(V_S, q_S) + \frac{g_c}{p} \cdot (V_D - V_S) + \frac{I_S}{p}\Big\} \quad (6)$$

$$\frac{dV_D}{dt} = \frac{1}{C_m}\Big\{ - I_{leak,D}(V_D) - I_{K-AHP,D}(V_D, q_D) - I_{Ca,D}(V_D, s_D) - \frac{I_{AMPA}}{1-p} - I_{K-C,D}(V_D, [Ca^{2+}]_D, c_D) + \frac{g_c}{1-p} \cdot (V_S - V_D) + \frac{I_D}{1-p}\Big\} \quad (7)$$

The maximal ionic conductances were chosen to be consistent with those in Traub's multicompartment model. In particular, the densities in our somatic compartment are consistent with the soma and proximal dendrite compartments of Traub's model and those in our dendritic compartment are consistent with those in the distal dendrite compartments of Traub's model. The values used are shown in Table 1. All other parameter values, set as in (Traub et al., 1991), are given in Table 2.

The model was implemented in Windows using XPPAUT, a differential equation simulation tool developed by B. Ermentrout. See Ermentrout (2002) for details. The Runge-Kutta fourth-order explicit method was used with a fixed timestep of 0.05 ms.

Table 1: Maximal ionic conductances (mS/cm^2)

Compartment	$\bar{g}_{Na,j}$	$\bar{g}_{Ca,j}$	$\bar{g}_{K-DR,j}$	$\bar{g}_{K-AHP,j}$	$\bar{g}_{K-C,j}$	$\bar{g}_{leak,j}$
Somatic ($j = S$)	30.0	6.0	17.0	0.8	15.0	0.1
Dendritic ($j = D$)	0.0	5.0	0.0	0.8	5.0	0.1

Table 2: Values and units of reversal potentials, coupling parameters, and membrane capacitance

Parameter	Unit	Parameter Value
V_{Na}	mV	120
V_{Ca}	mV	140
V_K	mV	-15
V_{leak}	mV	0
V_{EXC}	mV	60
g_C	mS/cm^2	1.5
p		0.5
C_m	$\mu F/cm^2$	3

2.1 Single cell model results

By injecting a sustained current into our somatic compartment (I_S) and later into our dendritic compartment (I_D), we reproduced behaviour found experimentally and obtained with the 19 compartment model of Traub et al. (1991). When a sustained current is applied to the somatic compartment, a steady train of somatic action potentials is produced with no bursting (Figure 2(a), cf. with Figure 12 of Traub et al. (1991)). The amplitude and frequency of both the somatic and dendritic voltage spikes are very similar to those obtained with Traub et al.'s 19 compartment model, which are consistent with experimentally observed values (Traub and Llinás, 1979). The interspike interval (i.e. the interval between action potentials) lengthens over time, which is consistent with

experimental findings for CA1 neurons (Lanthorn et al., 1984; Schwartzkroin, 1978; Traub and Llinás, 1979). When a current of the same strength is applied to the dendritic compartment, our model accurately simulates the dendritic calcium spike and somatic burst observed experimentally (Wong and Traub, 1982). The single burst is followed by a series of action potentials as seen in the simulations of Traub's 19 compartment model. These results are shown in Figure 2(b) (cf. Figure 12 of Traub et al. (1991)). The action potentials occur at a lower frequency than when the same current is applied to the somatic compartment. This is due to the increased calcium-dependent outward potassium channel ($I_{K-AHP,D}$) triggered by the large dendritic calcium spike, resulting in a longer afterhyperpolarization. For the simulations in Figure 2, we use a constant applied current of either I_S or $I_D = 1.25\ \mu A/cm^2$ (which translates to approximately $0.48\ nA$ in Traub's model), while the current in the other compartment is held constant at $-0.25\ \mu A/cm^2$. We have chosen this value so that it is slightly below the rheobase – the minimum amount of current required to excite the neuron – which is found to be approximately $-0.175\ \mu A/cm^2$ when $p = 0.5$. We did so in accordance with Traub et al. (1991), who applied a small negative current to suppress spontaneous firing. The coupling parameters are kept for now at the standard values of $g_C = 1.5\ mS/cm^2$ and $p = 0.5$. Keeping all other parameters fixed, spiking behaviour with physiologically reasonable frequencies was observed for $1.25\mu A/cm^2 \leq I_S < 3.5\mu A/cm^2$ and bursting behaviour was observed for $0.5\mu A/cm^2 \leq I_D < 4\mu A/cm^2$.

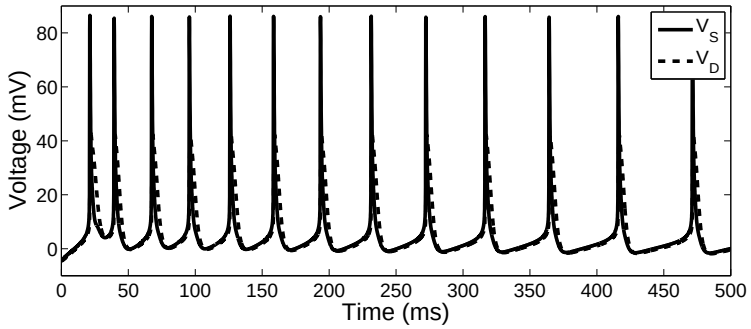

(a) A sustained somatic current of $I_S = 1.25\ \mu A/cm^2$ is applied

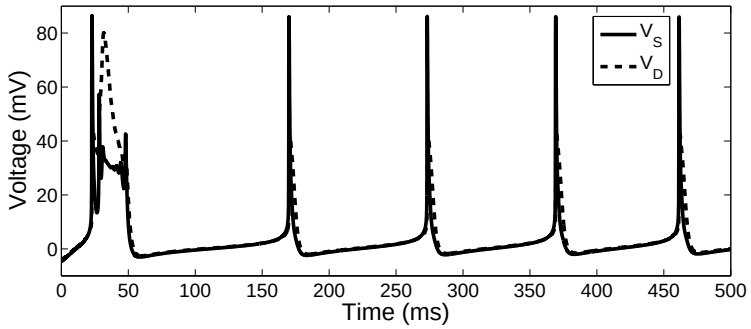

(b) A sustained dendritic current of $I_D = 1.25\ \mu A/cm^2$ is applied

Figure 2: The membrane voltage produced by the model when (a) a somatic and (b) a dendritic current is applied. Characteristic qualities of a CA1 neuron are reproduced: (a) a train of action potentials with increasing interspike interval, (b) a burst with a full dendritic calcium spike, followed by repetitive spiking.

As with Pinsky and Rinzel's (1994) CA3 model, our model only demonstrates the desired characteristic CA1 behaviour for a limited range of the coupling conductance, g_C. A very large coupling conductance essentially makes our model a single compartment model, and a very small g_C leaves us with isolated compartments. However, if g_C is slightly reduced then no bursting

occurs, and if g_C is slightly increased then aperiodic bursting occurs. Using an applied current of $I_D = 1.25\ \mu A/cm^2$, the desired bursting behaviour is reproduced for $1.35\ mS/cm^2 \leq g_C \leq 1.7\ mS/cm^2$.

2.2 Bursting mechanics

When a moderate sustained current is applied to the dendritic compartment, a somatic transient burst results (Figure 3(a)). To explain this burst qualitatively, we examine a single isolated model CA1 neuron with no synaptic input. Keeping the coupling parameters at their usual values of $g_C = 1.5\ mS/cm^2$ and $p = 0.5$, and maintaining $I_S = -0.25\ \mu A/cm^2$, a constant applied dendritic current of $I_D = 1.25\ \mu A/cm^2$ is used to create the initial burst followed by the action potential shown in Figure 3(a). We find that the interplay between the outward dendritic currents $I_{K-C,D}$ and $I_{K-AHP,D}$ with the inward dendritic current $I_{Ca,D}$ is the primary cause of bursting. Since the calcium-dependent potassium currents are essential to the bursting behaviour, we look at the associated variables $[Ca^{2+}]_S$, $[Ca^{2+}]_D$, q_S and q_D. In addition, the coupling parameters, g_C and p, are identified as key elements in generating this characteristic behaviour.

To determine why our model is much more likely to produce a single transient burst than repetitive bursting, we consider the dynamics of the outward potassium currents $I_{K-C,D}$, and $I_{K-AHP,D}$. Recall that the activation of the K-C ion channels depends both on the fast voltage-dependent gating variables, c_S and c_D, and on the slower intracellular calcium concentrations, $[Ca^{2+}]_S$ and $[Ca^{2+}]_D$. Therefore the time constant of this outward potassium channel largely depends on the slow decay time ($1/\beta_{[Ca^{2+}]}$) of the concentration of intracellular calcium. Similarly, the decay time of the potassium current $I_{K-AHP,D}$ depends on the slow gating variable q_D, which is also a function of $[Ca^{2+}]_D$. Thus the dendritic calcium spikes repolarize in accordance with the time constants of the slow variables $[Ca^{2+}]_S$, $[Ca^{2+}]_D$, q_S and q_D. During the burst, the length of the "quiet period" of V_S – when the soma is overdriven – is also determined mainly by these slow variables. From Figure 3(b) it is evident that the levels of q_S and q_D are low at the time of bursting, and are significantly elevated during the action potentials. High q values permit greater outward flow of I_{K-AHP}, allowing the voltage to recover faster, thereby reducing the probability of bursting. Similarly, the intracellular calcium concentration is low during the initiation of a burst (Figure 3(a)). An increased level of $[Ca^{2+}]$ activates the $K-C$ channels directly (and $K-AHP$ channels indirectly), permitting the compartmental voltage to repolarize faster. This faster recovery implies a decreased chance of bursting, resulting in single action potentials (Figure 3(a)). In contrast, a large dendritic calcium conductance, $\bar{g}_{Ca,D}$, creates a large inward calcium current flow. This makes it difficult for the outward potassium currents to counteract the inward flow, increasing the possibility of a burst.

The coupling parameters, g_C and p, play an essential role in generating bursts. Increased coupling results in increased flow of electrotonic current, elevating the q and $[Ca^{2+}]$ levels, as well as the inward current flow. Although the model will be more effective in creating the bursts, it will also recover faster, shortening the length of the burst. Thus, if the coupling parameter g_C is increased, the greater current flow between the two compartments will be more effective at initiating a burst. Similarly, the effects of the two compartments depend on their proportional size, p: the larger the dendritic compartment is compared to the somatic compartment, the more influence it will have.

3 Coupled Cell Model

When excited, the presynaptic neuron releases neurotransmitters into the synaptic cleft to signal its postsynaptic neighbour. According to Pinsky and Rinzel (1994) and Traub et al. (1992), the AMPA synapse is the dominant mechanism involved in the synchronization of two pyramidal neurons. Using this knowledge, we construct a standard AMPA synapse model (Destexhe et al.,

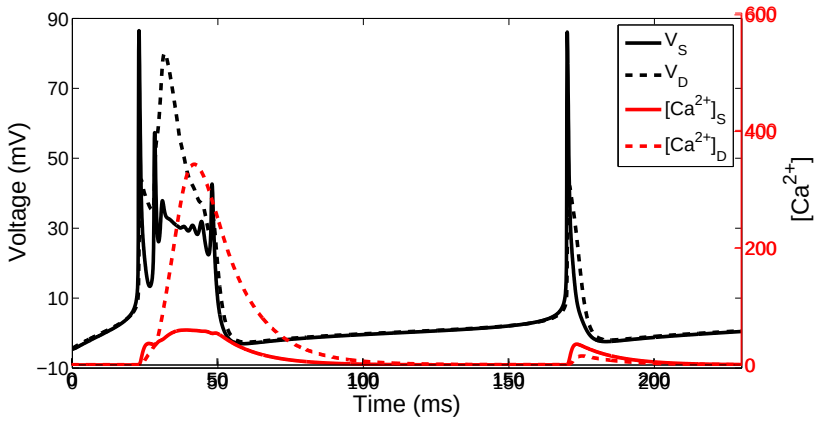

(a)

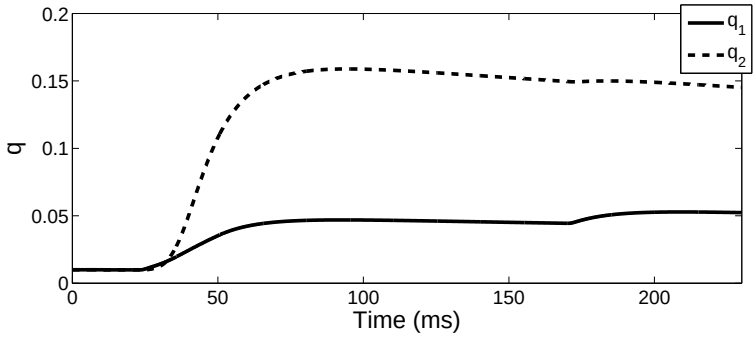

(b)

Figure 3: (a) The somatic and dendritic intracellular calcium concentrations, $[Ca^{2+}]_S$ and $[Ca^{2+}]_D$ (in red), overlaying the bursting and spiking. (b) q_S and q_D for the burst and spike sequence in (a). Therefore an applied dendritic current of $I_D = 1.25\ \mu A/cm^2$ results in the same voltage burst and spike. It is evident that increased levels of the slow variables $[Ca^{2+}]_S$, $[Ca^{2+}]_D$, q_S, and q_D decrease bursting activity. The characteristic transient burst occurs because of the initially low q values.

1998) which synchronizes coupled cell models under a strong connection, and desynchronizes the coupled models immediately once the strong connection is removed.

Since we have multiple cell models, we attach a subscript to our variables to denote the appropriate cell to which it belongs. Consider two cells, a presynaptic cell (cell 2) and a postsynaptic cell (cell 1). Using the gating variable W_1 and the maximal conductance $\bar{g}_{AMPA_1}$, we represent the synaptic current due to the AMPA receptors by:

$$I_{AMPA_1} = \bar{g}_{AMPA_1} W_1 (V_{D_1} - V_{EXC}) \tag{8}$$

where V_{D_1} is the voltage of the dendritic compartment of the postsynaptic cell, and the reversal potential of the excitatory synapse is given by $V_{EXC} = 60\ mV$ in accordance with Traub (1991). The presynaptic voltage is denoted V_{S_2} and V_{D_2} for somatic and dendritic voltage respectively. During a signal (or spike) from the presynaptic cell, the presynaptic voltage increases. If V_{S_2} surpasses some threshold, V_W, then the AMPA current of the postsynaptic cell activates with a time constant of 1 ms. Otherwise, the current will not activate. The activation degrades with a time constant τ_W. This is modelled via the following equation

$$\frac{dW_1}{dt} = H(V_{S_2} - V_W) - \frac{W_1}{\tau_W} \tag{9}$$

where H(x) is the Heaviside function: $H(x) = 1$ if $x \geq 0$, $H(x) = 0$ otherwise. We set $V_W = 40\,mV$ and $\tau_W = 2\ ms$ in accordance with Traub (1992) and Nadkarni & Jung (2005). To maintain a biologically realistic model, the two individual cell models should not be identical. Thus we alter some variables of "cell 2" slightly, while keeping them close to the values for cell 1.

3.1 Coupled cell results

Traub et al. (1991) stated that the AMPA synapse is primarily responsible for the synchronization of two neurons, and that when AMPA blockers are applied, the neurons are reported to desynchronize rapidly. To demonstrate that this characteristic is upheld in our model, we couple two cell models with an AMPA synapse and apply a constant input to the dendritic compartment of each cell. Cell 1 receives a stronger dendritic input than cell 2 and hence undergoes a longer burst and subsequently spikes at a faster rate that cell 2. With a weak AMPA connection the cells do not synchronize, but with a strong enough AMPA connection, they do. These results are illustrated in Figure 4

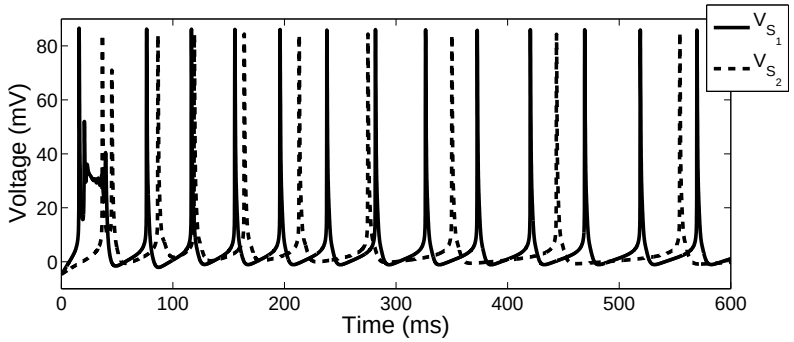

(a)

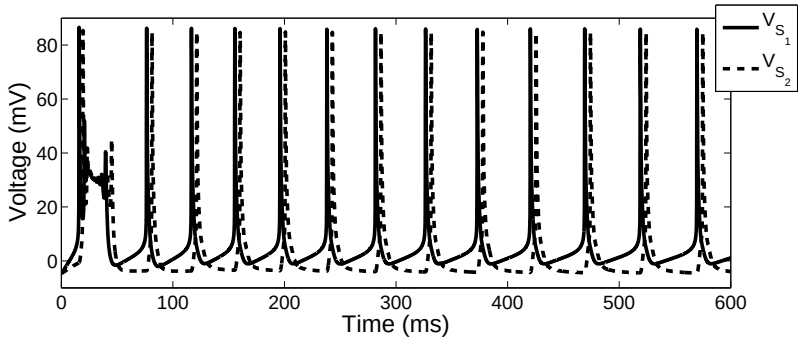

(b)

Figure 4: Cell 1 receives dendritic input $I_{D_1} = 2.0\mu A/cm^2$, cell 2 receives dendritic input $I_{D_2} = 1.25\ \mu A/cm^2$. (a) A weak AMPA connection: $g_{AMPA_2} = 0.04\ mS/cm^2$. (b) A strong AMPA connection: $g_{AMPA_2} = 0.2\ mS/cm^2$.

Similar results are obtained when the cells receive a sinusoidal input to the somatic compartment. We set the frequency and strength of the input to be different for both cell 1 and cell 2, so the cells do not synchronize on their own. If the neuron models are connected with a sufficiently strong AMPA conductance, then the cell with the weaker input will synchronize

to the cell with the stronger input. We show an example of these results in Figure 5, where the cells are connected strongly ($\bar{g}_{AMPA_1} = \bar{g}_{AMPA_2} = 0.2\ mS/cm^2$) until $t = 500\ ms$, and weakly ($\bar{g}_{AMPA_1} = \bar{g}_{AMPA_2} = 0.01\ mS/cm^2$) after $t = 500\ ms$. We set the input to be $I_{S_{cell1}}(t) = I_{S_1} sin(2\pi t/100) + 1$ so $I_{S_{cell1}}(t)$ fluctuates between -0.25 and 2.25. Similarly we set $I_{S_{cell2}}(t) = I_{S_2} sin(2\pi t/130) + 1$, so $I_{S_{cell2}}(t)$ has a slightly different period.

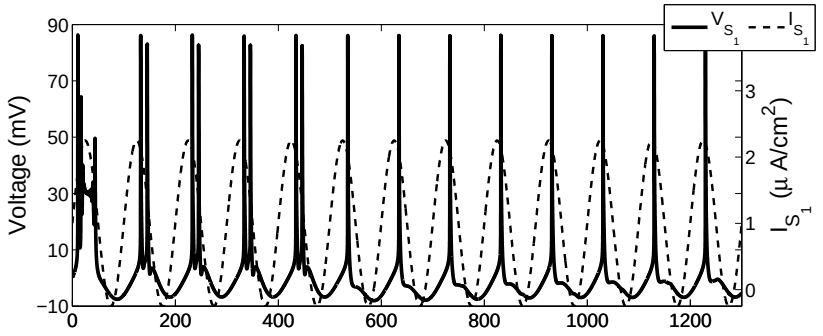

(a)

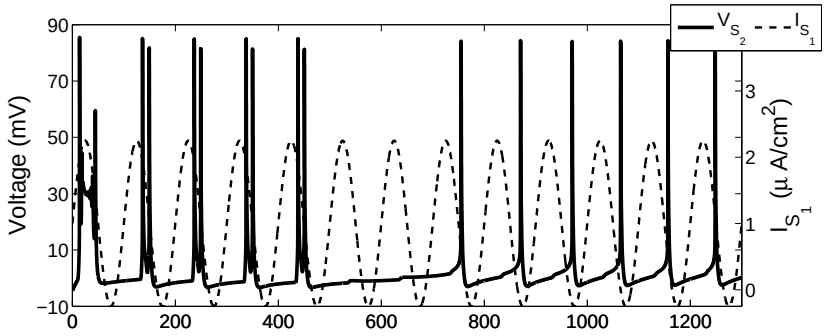

(b)

Figure 5: (a) The voltage of cell 1 and its corresponding input, $I_{S_{cell1}}(t)$. Note the synchronization to its input. (b) The voltage of cell 2 and the input from cell 1, $I_{S_{cell1}}(t)$. Cell 2 is synchronized to cell 1 until $t = 500\ ms$, at which point it desynchronizes. At $t = 500\ ms$ the connection goes from strong to weak, and the applied sinusoidal current to cell 2 dominates.

4 Discussion

Due to their susceptibility to excessive bursting and the organized nature of the hippocampal CA1 region, CA1 pyramidal neurons have been a focus of research involving seizure activity for many years (Traub and Llinás, 1979; Traub et al., 1991). Biophysical models of these neurons exist (Traub and Llinás, 1979; Traub et al., 1991), but for large networks or the analysis of key characteristics, a simpler model may be required. Thus, we created a two-compartment model of hippocampal CA1 neurons. The model reproduces qualitatively and quantitatively much of the characteristic behaviour of a CA1 neuron, as identified by Traub et al. (1991). That is, when the soma or proximal dendrites are stimulated with a current less than 1 nA ($I_S < 1\ nA$), a train of action potentials is exhibited. However, if the same current stimulates the distal dendrites ($I_D < 1\ nA$), a full dendritic calcium spike with somatic burst is produced, followed by low frequency action potentials. The bursting mechanisms were analyzed in detail, and the slow variables q and $[Ca^{2+}]$ were shown to influence the generation of a burst and the length of the interspike interval. It is clear from our analysis that a two compartment model is the minimal

conductance based model which can reproduce the appropriate bursting behaviour. The benefit of our simplified model is that key parameters involved in characteristic behaviour can be analyzed, and since it maintains its biological relevance, predictions about potential behavioural responses can be made. In addition, computational efficiency ensures that large networks can be created easily. As a first step toward such network models, we have implemented an AMPA synapse model and used it to investigate synchronization of two coupled CA1 neurons.

Acknowledgements

This work was supported by NSERC.

References

P. Andersen, R. Morris, D. Amaral, T. Bliss, and J. O'Keefe. *The hippocampus book*. Oxford University Press, New York, NY, 2007.

A. Destexhe, Z.F. Mainen, and T.J. Sejnowski. Kinetic models of synaptic transmission. In *Methods in Neuronal Modeling*, Cambridge, USA, 1998. MIT Press.

Bard Ermentrout. *Simulating, analyzing, and animating dynamical systems: a guide to XPPAUT for researchers and students*. Society for Industrial and Applied Mathematics, Philadelphia, P.A., USA, 2002.

T.H. Lanthorn, J. Storm, and P. Andersen. Current-to-frequency transduction in ca1 hippocampal pyramidal cells: slow prepotentials dominate the primary range firing. *Experimental Brain Research*, 53:431–443, 1984.

Paul F. Pinsky and John Rinzel. Intrinsic and network rhythmogenesis in a reduced Traub model for CA3 neurons. *Journal of Computational Neuroscience*, 1:39–60, 1994.

P.A. Schwartzkroin. Secondary range rhythmic spiking in hippocampal neurons. *Brain Research*, 149:247–250, 1978.

Roger D. Traub and R. Llinás. Hippocampal pyramidal cells: Significance of dendritic ionic conductances for neuronal function and epileptogenesis. *Journal of Neurophysiology*, 42(2): 476–495, March 1979.

Roger D. Traub, Robert K. S. Wong, Richard Miles, and Hillary Michelson. A model of a CA3 hippocampal pyramidal neuron incorporating voltage-clamp data on intrinsic conductances. *Journal of Neurophysiology*, 66(2):635–650, August 1991.

Roger D. Traub, Richard Miles, and György Buzsáki. Computer simulation of carbachol-driven rhythmic population oscillations in the CA3 region of the *in vitro* rat hippocampus. *Journal of Physiology*, 451:653–672, 1992.

S.F. Traynelis and R. Dingledine. Potassium-induced spontaneous electrographic seizures in the rat hippocampal slice. *J. Neurophysiology*, 59:259–276, 1988.

R.K.S. Wong and R.D. Traub. The dendrites and somata of hippocampal pyramidal cells generate different action potential patterns. *Society for Neuroscience Abstracts*, 8:412, 1982.

World Health Organization. Epilepsy: key facts. World Health Organization, 2009. URL `http://www.who.int/mediacentre/factsheets/fs999/en/index.html, 2009.` Available from http://www.who.int/mediacentre/factsheets/fs999/en/index.html, 2009.